

Principles of long-term fluids handling in paper-based wearables with capillary-evaporative transport

Cite as: Biomicrofluidics 14, 034112 (2020); doi: 10.1063/5.0010417

Submitted: 10 April 2020 · Accepted: 11 May 2020 ·

Published Online: 9 June 2020



View Online



Export Citation



CrossMark

Timothy Shay, Tamoghna Saha, Michael D. Dickey,^{a)} and Orlin D. Velev^{a)}

AFFILIATIONS

Department of Chemical and Biomolecular Engineering, North Carolina State University, Raleigh, North Carolina 27695-7905, USA

^{a)}Authors to whom correspondence should be addressed: odvelev@ncsu.edu and mddickey@ncsu.edu

ABSTRACT

We construct and investigate paper-based microfluidic devices, which model long-term fluid harvesting, transport, sensing, and analysis in new wearables for sweat analysis. Such devices can continuously wick fluid mimicking sweat and dispose of it on evaporation pads. We characterize and analyze how the action of capillarity and evaporation can cooperatively be used to transport and process sweat mimics containing dissolved salts and model analytes. The results point out that non-invasive osmotic extraction combined with paper microfluidics and evaporative disposal can enable sweat collection and monitoring for durations longer than 10 days. We model the fluid flow in the new capillary–evaporative devices and identify the parameters enabling their long-term operation. We show that the transport rates are sufficiently large to handle natural sweat rates, while we envision that such handling can be interfaced with osmotic harvesting of sweat, a concept that we demonstrated recently. Finally, we illustrate that the salt film deposited at the evaporation pad would eventually lead to cessation of the process but at the same time will preserve a record of analytes that may be used for long-term biomarker monitoring in sweat. These principles can be implemented in future platforms for wearable skin-interfacing assays or electronic biomarker monitors.

Published under license by AIP Publishing. <https://doi.org/10.1063/5.0010417>

I. INTRODUCTION

Paper-based microfluidic devices (often called “lateral flow assays”) have found numerous applications in recent years due to their low cost, manufacturing simplicity, and ease of use in point-of-care diagnostics. Paper is hydrophilic and porous, enabling it to wick small amounts of water, which is useful for biochemical analysis applications in which fluid volume is limited.¹ As the amount of research on paper microfluidics has grown, the sensing techniques and modalities have expanded spectaculary^{2–8} to biologically relevant analytes including glucose,^{1,9–13} lactate,¹⁴ nitrates,^{11,15,16} and cholesterol.¹⁶ These devices can be fabricated simply and efficiently by utilizing wax patterning,^{17,18} printing,^{9,12,15} lithographic,¹ and cutting methods.^{19–21}

One area where paper microfluidics can make a big impact is as a component of wearable devices that require long-term monitoring and management of small volumes of sweat or interstitial fluid (ISF).²² Long-term paper-based microfluidic sensing could not only find applications in fluid management for sweat sensing²³ but also

environmental monitoring,²⁴ drug compliance, and food quality control.³ Most existing paper-based devices are designed for one-time use only, functioning under relatively intense capillary flow into the paper, which ceases upon saturation. Researchers have begun exploring how they can control the rate of capillary wicking into paper-based devices to prolong sensing duration or incorporate areas of mixing and separation.^{25,26} Flow control has been achieved through various geometrical designs in both 2D and 3D.^{27–31} However, flow terminates after the paper has been fully saturated, thus reducing the capillary pressure necessary to drive subsequent flow. This problem may be addressed through evaporation of some of the collected liquid. Traditional microfluidic devices (i.e., those that do not use paper) have utilized evaporation at openings at the end of a microchannel to drive fluid flow.^{32,33} One device has facilitated pumping by evaporation from a paper plug at the outlet of a microfluidic channel.³⁴ Microfluidic pumps have been inspired by the evaporation occurring in trees,³⁵ and such evaporation assisted capillary wicking has even been utilized to concentrate biomarkers.³⁶

The monitoring of human health and well-being with the use of wearables is considered critical in the next generation of biomedical devices. The field of wearable sensors from sweat collection and analysis has seen a number of impressive and rapid advances in the past few years.^{23,37–47} These technologies presently face a key challenge—the need to passively manage sweat over long durations of collection. A microfluidic paper platform capable of generating and managing stable long-term fluid flows could become an integral component in the next generation of sweat sensing devices. We evaluate the feasibility and efficacy of a platform for continual long-term pumping of fluids, such as sweat, using capillary–evaporative pumping through paper microfluidics.

The long-term pumping of fluids requires a long-term source of fluids. Thus, another major problem that needs to be solved for achieving long-term sweat collection and monitoring by such devices (e.g., in the format of wearable skin patches) is the collection of sweat under conditions of normal human activity, which only rarely involves profuse sweating. Our group demonstrated a new concept of osmotic fluid collection and withdrawal by a method based on the osmotic pressure difference between the model sweat and a hydrogel disk with higher solute concentration than sweat.⁴¹ The difference in the chemical potential created by the hydrogel readily pulls the model biological fluid across a dialysis membrane, using the difference in chemical potential in lieu of mechanical pumping.⁴⁸ Recent reports also illustrate the potential of gels in capturing sweat for hydration monitoring.⁴⁹ Merging such fluid extraction principles with paper microfluidics can potentially lead to a huge advancement in the area of non-invasive sweat sampling and management. The development of long-term skin sweat assays is an ongoing area of research in our group, and the study here represents one component of that work.

This report presents a detailed analysis of how paper microfluidics can function as a key part of a platform for long-term sweat sampling and biomarker monitoring. We conceptualize how the joint action of capillary wicking and evaporation can sustain continuous and long-term withdrawal of fluid containing dissolved solutes similar in composition to sweat. We first show that paper strips of controlled geometry can passively pump fluid for sensing purposes for long durations. Modeling and experiments both show how the strip geometry can control the flow. We then evaluate the limitations of evaporative pumping based on hydrodynamic resistance and salt accumulation for long-term use. Finally, we explore how such paper microfluidic platforms can be deployed for colorimetric sensing as a model of biomarker quantification in biofluids.

II. EXPERIMENTAL

A. Materials

Whatman quantitative filter papers, hardened, ashless Grade 542 (GE Healthcare Life Sciences), were used as the wicking strips in the device conduits. The strip designs were created in CorelDraw, and the paper strips were cut on a CO₂ laser cutter (Universal Laser Systems VLS 3.5). The body of the device was fabricated using polydimethylsiloxane (PDMS, Dow Corning). Yellow fluorescent dye (Tracerline, TP39000601) was dissolved in phosphate buffer saline (PBS) to mimic a model sweat biomarker. PBS has an ionic strength of $\approx 0.15\text{M}$.

B. Paper microfluidic device setup

As shown in Fig. 1, the paper microfluidic device consists of three main components: a sampling interface where the paper is in contact with the desired fluid, a linear strip of paper that wicks the fluid, and an open large surface area where the evaporation takes place at the end of the fluid path. The paper cutouts were placed on an acrylic sheet to keep them flat and block evaporation from one side of the paper. The other side of the paper strip was encased by a slab of PDMS. A small portion (1 cm long) of the paper segment extended from this sandwiched structure, serving as the sampling zone for receiving fluids, including model sweat.

C. Flow monitoring procedures

The entire assembly was mounted vertically. To help visualize the flow, we placed a black mat behind the acrylic plate. A Canon EOS Mark5 DSLR camera focused on the paper strip and images were taken at the exposure of 1/13th s. Six UV LED lights, from an ACLOROL 5050 LED strip, were placed approximately 2 in. in front of the paper strips to illuminate the fluorescent dye. An enclosure surrounded the setup to block external light from affecting the images. The camera recorded time-lapse images every 30 s to follow the fluorescent dye motion through the paper. All tests were performed in ambient lab conditions [$\sim 22^\circ\text{C}$ and 40% relative humidity (RH)].

The strips were initially suspended in air with the sampling region interfacing de-ionized (DI) water to allow for wicking to fully wet the strip. Once fully wetted, the collection pad was brought in contact with a fluorescent solution and the motion of the dye was tracked. Depending on the test performed, the sampled solution may be switched between DI water and solutions with varying dye concentrations. For long duration tests, the paper strips were kept in contact with PBS solution continually over the 10-day span. Fluorescent dye was introduced as stated above once a day in order to obtain flow data. Matlab was used to extract quantitative data from the series of images (Fig. S1 in the [supplementary material](#)).

III. RESULTS AND DISCUSSION

The key aspects of device construction and operation reported here are illustrated in Fig. 1. There are two distinct zones along the paper channel—a thin long rectangular section directly interfacing the analyte solution and a broad circular arc region (evaporation pad) with a high surface area. During the initial stage of operation, capillary wicking draws fluid from a sampling region (which in a wearable device implementation would be skin) and transports it through the paper strip to the evaporation pad. Evaporation takes over as the dominant pumping force after saturation of the paper pad. Capillary action replenishes evaporated fluid in the pad, creating a pull that continually draws fluid from the sampling region through the channel to the evaporating pad. This enables the paper device to pump for long durations after the fluid wets the paper.

One application of such devices would be non-invasive and continuous sweat withdrawal, where the paper microfluidic channels can be incorporated into a device, backed by a hydrogel disk infused with a liquid of high solute concentration. On interfacing

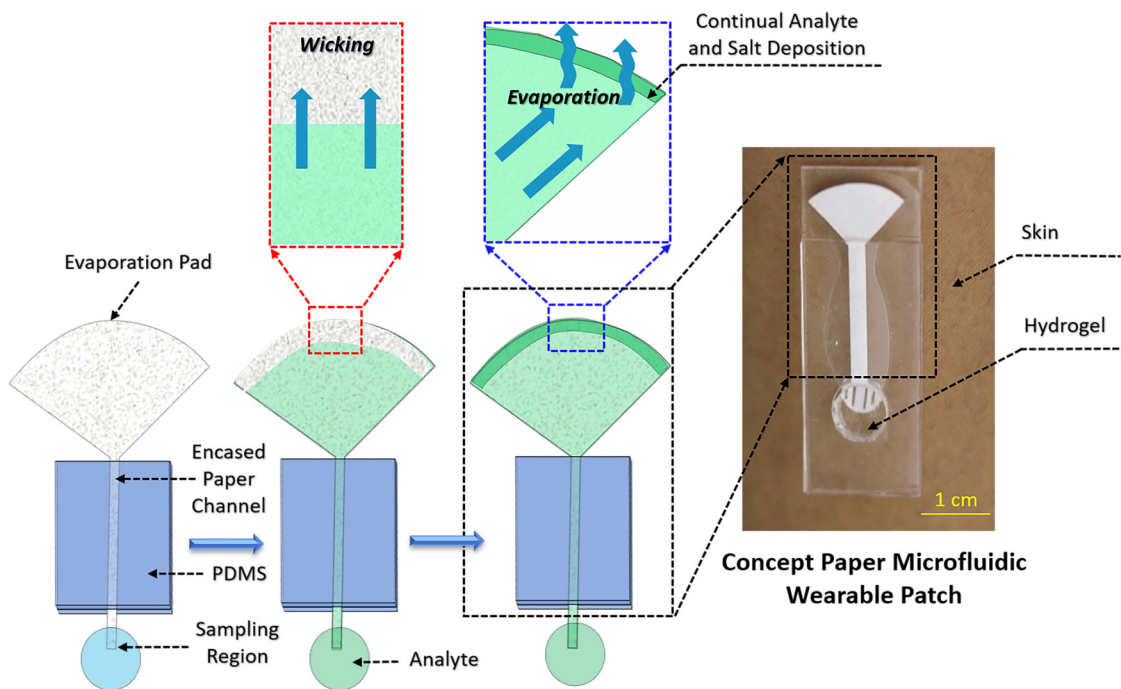


FIG. 1. Schematic of the working principle of the paper-osmotic microfluidic device. Paper strips are fabricated with three sections: a section that samples fluid, an encased paper channel for transporting fluids, and a paper pad with a large surface area that utilizes evaporation to continually drive fluid through the device. Wicking initially saturates the paper. Evaporation then removes water from the pad, allowing for capillary action to pump more fluid through the channel to this pad. The evaporating model biofluid leaves behind a deposit of dried salts, which over time impedes the device operation. The photo on the right illustrates a prototype of a skin-interfacing patch assay, where this principle is used for collection of sweat via an osmotic hydrogel interface.

such a device with skin, the chemical potential difference between the hydrogel disk and the skin would initiate fluid withdrawal from the skin,^{41,49} which would then wick along the paper channel and eventually get disposed into the evaporation pad. The pad can be used for quantifying the various associated biomarkers. However, an in-depth analysis about the biomedical application of such devices is beyond the scope of this study.

A. Visualizing and characterizing the flow of water

We first used a fluorescent dyed water solution to visualize and trace fluid movement through the paper. The sampling region of the paper strips interfaced a reservoir of DI water. During this initial priming stage, capillary action wicked water to fully wet the strip. After saturating the strip with water, we switched the solution in the reservoir every 20 min between a commercially available fluorescent dye and DI water. We measured the flow rate by monitoring the intensity of the alternating bands of fluorescent dye that passed through the paper. The continual transport of fluid is visualized in Fig. 2(a) via the movement of the bands of green fluorescent dye (Video S1 in the [supplementary material](#)). The fluorescence intensity of the dye was measured digitally from the images at the locations denoted by the red and blue dotted lines and plotted vs time by using Matlab (Supplementary Note 1 in the

[supplementary material](#)). The resulting signal is in the form of periodic peaks correlated with the presence or absence of the dye in the reservoir [Fig. 2(b)].

The distance between two colored intensity signals in Fig. 2(b) is proportional to the time it takes for the dye to travel the distance between the two points of measurement. The flow velocity of the wicking in the channel was evaluated by the distance between the two peaks divided by the time difference between the two sequential signals. These data show that the paper devices with evaporative water disposal have a steady state flow rate over time scales longer than hours. Even after saturating the paper, the fluid continues to maintain stable flow rates that do not diminish over 2 h, as shown in Fig. 2(c). We verified the evaporative pumping mechanism through tests in settings of variable humidity and by observing the temperature drop in the pad associated with evaporation (see Figs. S2 and S3 and Supplementary Note 2 in the [supplementary material](#)).

B. Velocity model and geometry limits

The flow characteristics of this simple class of paper devices depend on their geometry. The time delay between the first moment a target analyte contacts the paper to the time it reaches the sensing area is determined by the geometrical design of the

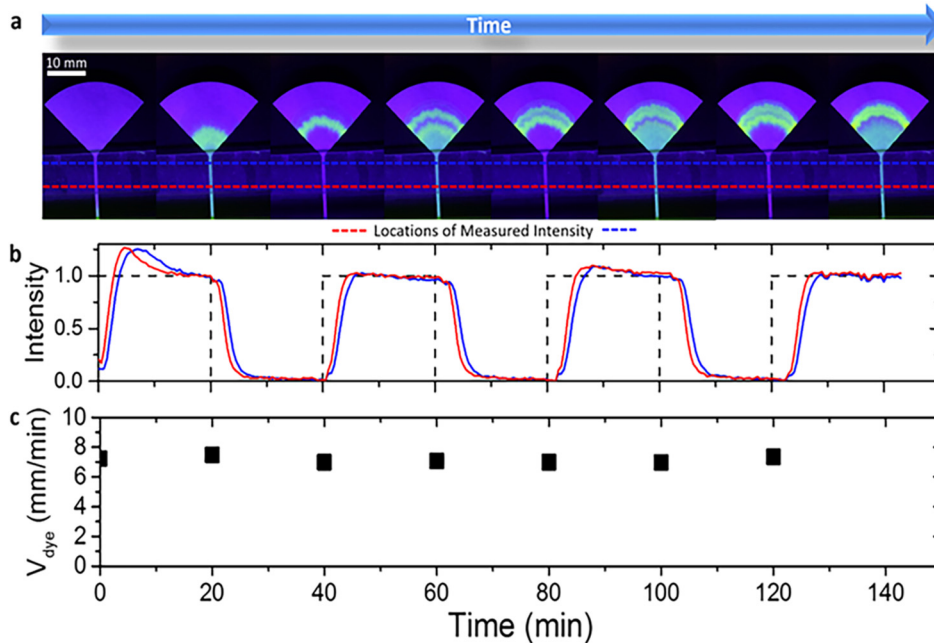


FIG. 2. (a) Images of a paper strip during testing where the sampled fluid was periodically exchanged between DI water and a fluorescent dye every 20 min. The corresponding time-lapse video can be seen in Video S1 in the [supplementary material](#). (b) Image analysis shows that the intensity of the dye oscillates in the encased channel as the bands of dye are transported towards the evaporation pad. One measurement was performed at the bottom of the channel (red dotted line) and the other was measured near the top of the channel (blue dotted line). (c) The velocity of the dye was calculated at each step. Note that the flow remains constant over a 2 h span.

paper channel, including the area of the evaporation pad and the width and length of the paper “channel” connecting the collector and evaporation pad. We measured the dye velocity through the paper conduits connecting to varying evaporation pad areas and channel widths. The data were interpreted based on a generalized fluid transport model that accounts for three key factors: (1) evaporation rate based on pad size, (2) velocity of dye through the paper channel based on channel geometry (cross-sectional area), and (3) chromatographic effects between the dye and paper substrate. It also allowed us to identify the limitations of the total fluid flow rate that arise from the hydrodynamic resistances encountered throughout the paper channel.

To evaluate the evaporation rate, we assume that there is a constant evaporation flux [H (mg/cm² s)] over the entire area (A) of the evaporation pad, as capillary action will keep the paper wetted. The mass flow rate of water (\dot{m}) through the device is calculated as $\dot{m} = HA$. The flow rate of water through the paper channel in the microfluidic device can be obtained from a mass balance using the fluid velocity (v), channel width (w), and moisture content of the wet paper [M (mg/cm²)]. This results in a mass flow of $\dot{m} = vwM$.

Chromatographic effects arising from the dye adsorption-desorption equilibria between the dye molecules in the fluid and paper substrate result in the lagging of dye behind the fluid. This lag can be taken into account by using a retardation factor (R_f), which correlates the dye velocity with the actual velocity of fluid traveling through the paper microfluidic channel.

At steady state of complete device saturation with water, the mass of the evaporated water per unit time equals the mass flow rate through the channel. Incorporating the retardation factor and rearranging the equation result in an expression for dye velocity. This model, plotted in Fig. 3(a), fits the data well without any

fitting parameters (as the value of R_f was measured independently),

$$v_{dye} = \frac{R_f HA}{wM}. \quad (1)$$

Another flow regime is established when the water does not completely saturate the evaporation pad. Increasing the area of the pad increases the flow rate up to the point where the flow resistance of the channel limits the maximum flow rate. The flow rate in this regime is established by the rate at which capillary wicking of fluid through the device can replenish the evaporated fluid. The fluid transport through the paper channel encounters hydrodynamic resistance, which induces an associated pressure drop. Balancing this hydrodynamic pressure drop with the capillary pressure defines the maximum flow rate achievable through the channel. The pressure drop (ΔP) over the channel length (L) can be correlated to the maximum flow rate of water [Q_{max} (m³/s)] through the paper device, viscosity (μ), permeability (κ), and thickness (h) using Darcy's law,⁵⁰

$$\frac{\Delta P}{L} = -\frac{\mu}{\kappa wh} Q_{max}. \quad (2)$$

We assume that the pressure drop of the fluid in the evaporating pad is negligible due to its much larger cross-sectional area. The maximum flow rate is then limited by the maximum capillary wicking rate and equal to the flow rate expected from evaporation,

$$Q_{max} = \frac{\Delta P wh \kappa}{\mu L} = \frac{HA_{max}}{\rho}. \quad (3)$$

A re-arrangement of this equation makes possible to evaluate the maximum wetted area (A_{max}) for a given channel width while

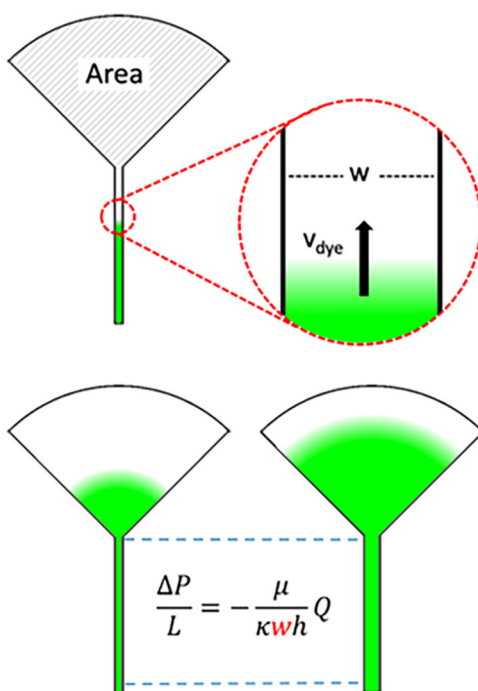
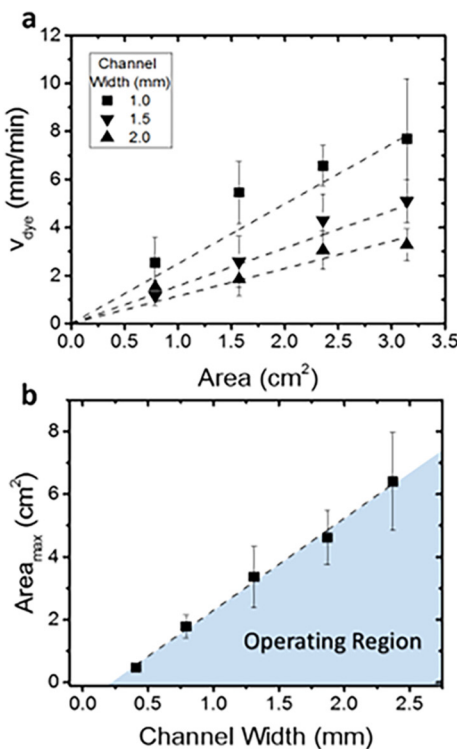


FIG. 3. (a) Plot of the measured dye velocity in the paper channel relative to the size of the evaporation pad for various channel widths. Velocity increases with increased area and decreased channel width, as expected. The theoretical model, shown on the right, was plotted for each channel width and shows agreement with the measurements. (b) Plot showing the maximum wetting area achieved on the evaporation pad vs the channel width. Smaller channel widths have a higher pressure drop, which hinders the flow of fluid through the channel and reduces the maximum wetted area of the evaporation pad. All data bars represent the standard deviation.

the device is operating at its steady state,

$$A_{max} = \left(\frac{\Delta Ph\kappa\rho}{\mu L H} \right) w. \quad (4)$$

We measured the maximum area of water coverage A_{max} at varying channel widths and sizes of the evaporating pads. The results are plotted in Fig. 3(b). The maximum wetted area follows a linear relationship with channel width as predicted by the model. The deviation from the origin may be due to the neglected pressure drops in the evaporating pad or evaporation from the channel. The observed flows are comparable to a previous report on fluid transport in paper devices with fan geometry.⁵¹

This graph defines the parameter region where the device operates at maximal efficiency, when the evaporation pad is completely wetted [shaded area in Fig. 3(b)]. Operation with evaporation pads having larger areas above this line is suboptimal, as the pad is not fully saturated, since capillary wicking is not able to replenish water rapidly enough to fully saturate the pad area. Pads with smaller evaporation areas can operate reliably as capillary action is able to fully replenish the evaporated water. Points along the line represent an exact balance of capillary flow and evaporation. These results reveal the flow-based limitations with evaporation-based pumping through a porous paper device.

C. Long-term operation with isotonic salt solutions

One key application of such devices that we foresee is transport for analysis of biological media such as sweat or interstitial

fluid. In this context, they should operate for long periods of time with biological solutions that contain dissolved salts and other species. These solutes will accumulate on the evaporation pad over time and will precipitate when their concentration exceeds the solubility limit. The caked salt deposits will suppress the fluid evaporation from the pad because of the increased osmotic pressure from higher salt concentration as well as physical obstruction from the precipitated salt crystals on the paper. Thus, the limits of pumping hindered by salt deposition were examined to determine the maximum operating lifetime.

We evaluated the limits of long-term operation of the paper strip devices fed with PBS to observe the effects of salt accumulation on flow rate. PBS was used to simulate biological and medically relevant body fluids, such as sweat, which have the same ionic strength. The evaporative pumping of PBS results in the visible formation of a precipitated layer of salts at the outer edge of the evaporation pad. Interestingly, the growth of this layer was gradual and slow. A solid salt layer is observed at the evaporation pad periphery by the second day of testing [Fig. 4(a)]. The solid salt crust grew inward from the evaporation pad periphery toward the center each day as more salt precipitated [Fig. 4(b)]. However, in spite of the slow deposition of salt crust, the pumping process continues to operate for several days.

The area available to evaporate water for pumping decreases over time as a direct result of salt accumulation. Dye velocity is proportional to the evaporating area, as shown in Eq. (1). The salt accumulation slowly suppresses the flow rate, and both dye velocity and uncovered area decrease over time as salt accumulates. The

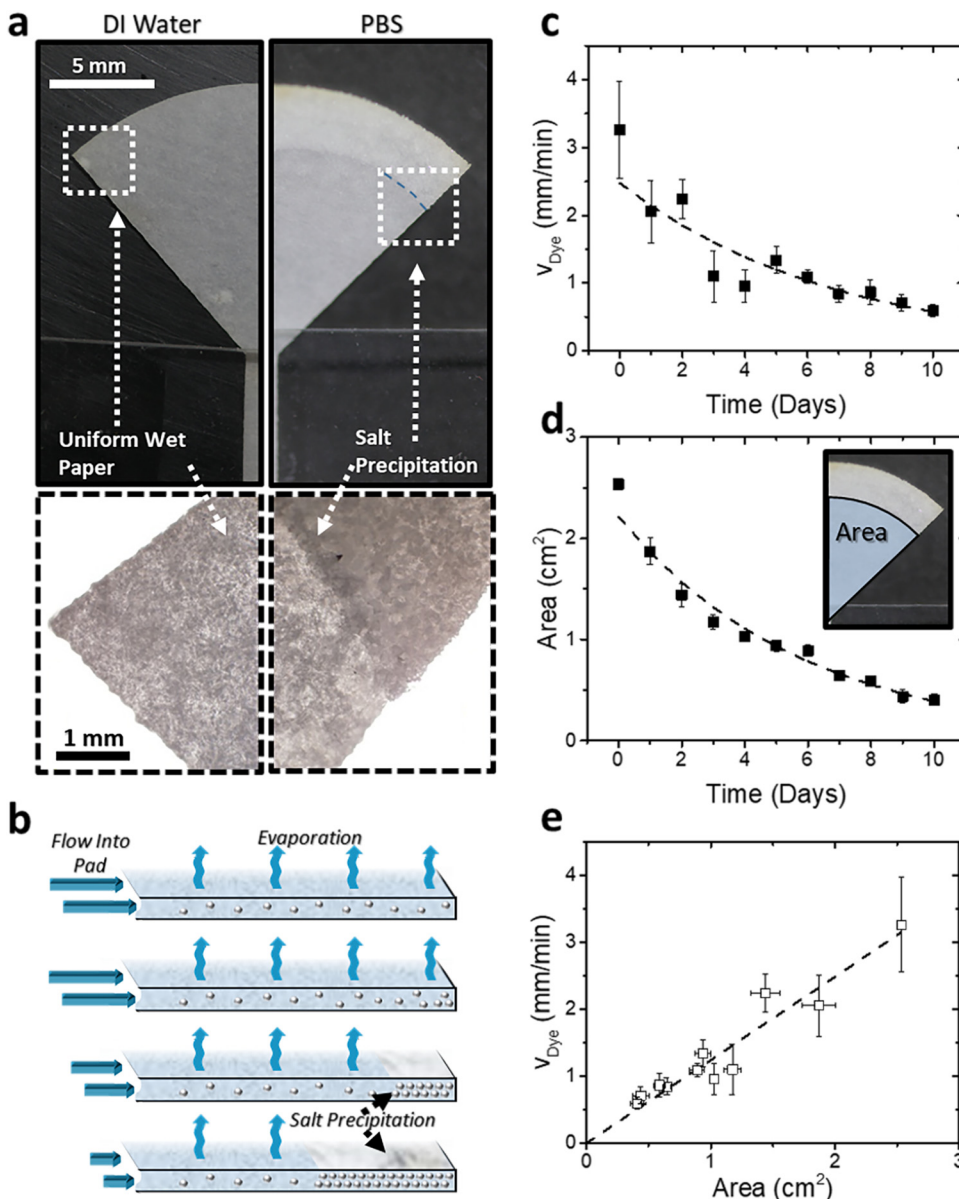


FIG. 4. (a) Images and micrographs showing the evaporating pad of the paper strip under operation of DI water and PBS. Salt deposits from the PBS accumulate at the periphery of the pad over time as water evaporates. (b) Schematic showing the mechanism of salt accumulation. The salt deposit begins to build up at the edge of the pad, resulting in a front of salt crystals moving inward from its edge. (c) Velocity of a fluorescent dye was measured over a 10-day span to determine the effect of salt accumulation on fluid flow. (d) The area of the paper pad not covered by salt crystals was measured over this span. Both velocity and area show a negative exponential decay over time. (e) Velocity plotted vs the area available for evaporation, delineating two evaporation regimes.

decrease in the evaporation rate due to an increase in concentrated and precipitated salt is broadly analogous to that of the evaporation of saline water from soil.⁵² The correlations that relate fluid velocity, area, and time are $v = \alpha_1 A$ and $dA/dt = -\alpha_2 v$, where α_i are constants. The solutions of this system of first order differential

equations is in the form of exponential decay functions,

$$v = v_0 e^{-\frac{t}{\tau}}, \quad (5)$$

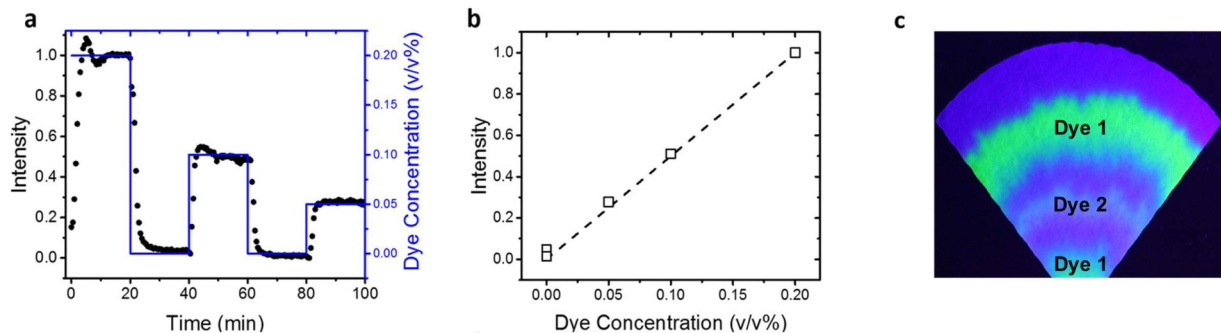


FIG. 5. (a) Plot showing measured intensity of dye in a paper channel [black circles, measured at the same location as Fig. 2(a)] while adjusting the concentration of dye in the solution reservoir via step changes (as shown by the blue plot). (b) Intensity plotted vs dye concentration demonstrates the expected linear correlation. (c) “Tree ring” pattern formation on evaporation pad due to the accumulation of multiple dyes and salts for more than 5 h of operation.

$$A = A_0 e^{-\frac{t}{\tau}}. \quad (6)$$

To evaluate the long-term device performance, we measured the dye velocity over a 10-day span [Fig. 4(c)]. Concurrently, we recorded the area of the evaporation pad not covered in salt crystal cake where the evaporation of the water medium was taking place [Fig. 4(d)]. The data are in good agreement with Eqs. (5) and (6). Both velocity and area of salt-free region demonstrate exponential decay over a period of 10 days [Figs. 4(c) and 4(d)]. The velocity and area remain linearly correlated with each other [Fig. 4(e)]. Integration of the velocity over time shows a total fluid uptake of ~ 13 ml of solution, which would deposit ~ 115 mg of salt. Thus, evaporation disposes nearly 500 times the volume of liquid held by a saturated paper strip of this size (0.025 ml). To put this in perspective of human perspiration, an area of 1 cm^2 skin of the forearm would produce an average sweat rate of roughly $0.75\text{ }\mu\text{l}/\text{min}$.⁵³ Assuming continuous sweating at this average sweat rate, it would take nearly 290 h (more than 12 days) before 13 ml is pumped and enough salt has precipitated to hinder the evaporative flow. This result shows that passive evaporative disposal of the sweat released by human skin under normal conditions could, in principle, operate for more than 10 days, a few orders of magnitude longer than typical operational times of state-of-the-art wearable microfluidic systems. Overall, the design of the paper channel provides a new universal platform that can serve for both continuous and non-continuous sensing (on the pad).

D. Dynamic and static solute profiles during device operation

The use of devices in continual monitoring of chemical and biological markers requires predictable solute transport and fidelity of the concentration profile during the fluid transport as investigated above. In addition, the fate of the analyte deposited on the evaporation pad is of specific interest, as within a specific time interval, the mass of the solute accumulated on the drying pad could be expected to represent the integral amount of all material transported through the paper strip “channel.” Thus, the mass transport in the continual pumping paper microfluidic devices was

followed to establish the dynamic and overall concentration profiles of the analyte simulant.

Solutions with varying dye concentration (0%–0.2%) were wicked through the paper channel, while their fluorescence intensity profiles were measured over time. These tests were performed using multiple concentration step changes as shown in Fig. 5(a). They showed how the response of the measured intensity to the change in sampled dye depends on the pumping rate and channel width. The steady state intensity was used to create a correlation curve with the dye concentration [Fig. 5(b)]. There is a linear relationship between color intensity and dye concentration. This correlation was expected, as concentration of the dye was the only parameter altered and was directly correlated to color intensity. This result demonstrates the ability of this pumping device to be used for colorimetric sensing applications.

One important observation is that analogous to the accumulated salt-ring in Fig. 4(b), the steady flow and continuous evaporation of the dye solution from the pad also results in dye embedding in “tree ring” deposits from caked salt that keep on progressing inward toward the center over time and continue until the pad fully is fully saturated with dry salt [Fig. 5(c)]. This linear progression of these deposits and uniform pattern of rings is a result of the pad geometry and laminar flow of the inflowing dye solution. Thus, the evaporation pad can potentially function as a useful repository for analytes in sweat by maintaining a time-stamped record of their concentration. It is expected that the embedding of biomarkers and other organic molecules of interest such as drug metabolites within a dry salt layer could serve as a reasonable way to preserve the record for later analysis.

IV. CONCLUSIONS

Microfluidic devices based on paper can be easily fabricated and have become a major platform for making simple, inexpensive, and convenient biological and medical assays. The data summarized here show how paper-based devices may find application in technologies for non-invasive health and wellness monitoring from skin due to their ability to continually pump fluid with composition similar to sweat for long durations via evaporation. Here, we

used a reservoir of model fluid, but as a next step, we plan to combine these devices with our earlier osmotic gel patches⁴¹ to explore this concept on human skin. The data and models show that the paper geometry—both the linear flow strip and pad—controls the flow rate of fluid through these devices. The ability to pump model sweat continuously for 10 or more days addresses a limitation of present sweat sensing devices, which collect sweat from the body but do not have a way of handling that fluid for long term after testing has been performed. The demonstrated long-term performance of these paper-based devices make them suitable to be interfaced with skin sweat collection interfaces based on osmotic gel patches,⁴¹ as well as sweat released by physical exertion^{38,39,42,54–57} or by iontophoretic extraction using sweat stimulating agents.^{58,59} The paper strip can serve as a site for hosting electrochemical sensors,⁶⁰ although the detection will occur after a time lag on the order of minutes. Another interesting, although more challenging, opportunity is to combine this transport and monitoring principle with devices that monitor interstitial fluid (ISF), which can be withdrawn by means of microneedles.²² This will require further consideration of the osmotic effects and engineering of the transport at the microneedle–paper interface.

The pumping mechanism in the evaporation-based paper devices requires no external power and thus can be used for continual long-term monitoring in wearable devices where power consumption may be limited. Such devices involving evaporation would not operate at a relative humidity of 100% (saturation conditions) as they need water evaporation. However, an argument can be made that humans rarely operate for long in such environments and would profusely sweat in such conditions, making sweat collection straightforward. Finally, as such a device would be in constant contact with the human skin, they would experience only small variations in temperature, which is needed for calibration of some biosensors and assays.

Another interesting capability revealed by the data is the potential of long-term recording of the analyte profile. The results for the sequential introduction, detection, and “tree ring” layering of the fluorescent model analytes highlight the strictly laminar fluid flow in the paper channel and evaporation pad. This layered accumulation of salts preserves and vitrifies the analytes, which could be analyzed later either by a scanning device, reproducing a time profile of a biological marker/drug that can appear in the sweat (similar to the analysis of tree rings or layers of each to provide chronological information), or using conventional colorimetric assays. Thus, these devices could report both a near-real time reading by a biosensor (which could be integrated in the “straight” portion of the paper device) or record a long-term temporal profile of sweat composition sequentially deposited by the laminar flow along the evaporation pad.

The simple capillary-assisted evaporative pumping platform, the principles of which are shown here, may be able to present an integral part of the next generation of wearable technologies. These principles in the near future will be subject to biomedical validation of biological analytes with patches on human skin. Overall, even at this point, the results show how capillary wicking and evaporation in paper microfluidic channels, in conjunction with osmotic gel withdrawal, could form the basis of new platforms for devices with non-invasive, passive long-term continuous sweat withdrawal and management.

SUPPLEMENTARY MATERIAL

See the [supplementary material](#) for more graphical and numerical data, analysis, and a movie illustrating the operation of the model microfluidic devices.

AUTHOR'S CONTRIBUTIONS

O.D.V. and M.D.D. conceived the idea and designed the project. T. Shay performed the fluid flow experiments and developed the flow model. T. Saha designed and carried out detailed model experiments. T. Shay and T. Saha analyzed the results and plotted the data and schematics. All authors contributed to the manuscript.

ACKNOWLEDGMENTS

We gratefully acknowledge the funding of this study by the NSF-ASSIST Center for Advanced Self Powered Systems of Integrated Sensors and Technologies (No. EEC-1160483). We are thankful to our colleague Michael Daniele for insightful advice and assistance.

DATA AVAILABILITY

The data that support the findings of this study are available within the article [and its [supplementary material](#) experiments]. Further details can be obtained from the authors upon request.

REFERENCES

- ¹A. W. Martinez, S. T. Phillips, M. J. Butte, and G. M. Whitesides, *Angew. Chem. Int. Ed.* **46**, 1318 (2007).
- ²A. W. Martinez, S. T. Phillips, E. Carrilho, S. W. Thomas III, H. Sindi, and G. M. Whitesides, *Anal. Chem.* **80**, 3699 (2008).
- ³Z. Nie, C. A. Nijhuis, J. Gong, X. Chen, A. Kumachev, A. W. Martinez, M. Narovlyansky, and G. M. Whitesides, *Lab Chip* **10**, 477 (2010).
- ⁴W. Dungchai, O. Chailapakul, and C. S. Henry, *Anal. Chem.* **81**, 5821 (2009).
- ⁵W. Zhao and A. V. D. Berg, *Lab Chip* **8**, 1988 (2008).
- ⁶A. K. Yetisen, M. S. Akram, and C. R. Lowe, *Lab Chip* **13**, 2210 (2013).
- ⁷D. D. Liana, B. Raguse, J. J. Gooding, and E. Chow, *Sensors* **12**, 11505 (2012).
- ⁸Q. Cao, B. Liang, T. Tu, J. Wei, L. Fang, and X. Ye, *RSC Adv.* **9**, 5674 (2019).
- ⁹W. Dungchai, O. Chailapakul, and C. S. Henry, *Analyst* **136**, 77 (2010).
- ¹⁰J. Yu, L. Ge, J. Huang, S. Wang, and S. Ge, *Lab Chip* **11**, 1291 (2011).
- ¹¹S. A. Klasner, A. K. Price, K. W. Holeman, R. S. Wilson, K. J. Bell, and C. T. Culbertson, *Anal. Bioanal. Chem.* **397**, 1821 (2010).
- ¹²K. Abe, K. Suzuki, and D. Citterio, *Anal. Chem.* **80**, 6928 (2008).
- ¹³J. Lankelma, Z. Nie, E. Carrilho, and G. M. Whitesides, *Anal. Chem.* **84**, 4147 (2012).
- ¹⁴W. Dungchai, O. Chailapakul, and C. S. Henry, *Anal. Chim. Acta* **674**, 227 (2010).
- ¹⁵X. Li, J. Tian, G. Garnier, and W. Shen, *Colloids Surf. B Biointerfaces* **76**, 564 (2010).
- ¹⁶A. W. Martinez, S. T. Phillips, Z. Nie, C.-M. Cheng, E. Carrilho, B. J. Wiley, and G. M. Whitesides, *Lab Chip* **10**, 2499 (2010).
- ¹⁷H. Yagoda, *Chem. Anal. Ed.* **9**, 79–82 (1937).
- ¹⁸E. Carrilho, A. W. Martinez, and G. M. Whitesides, *Anal. Chem.* **81**, 7091 (2009).
- ¹⁹E. M. Fenton, M. R. Mascarenas, G. P. López, and S. S. Sibbett, *ACS Appl. Mater. Interfaces* **1**, 124 (2009).
- ²⁰E. Fu, P. Kauffman, B. Lutz, and P. Yager, *Sens. Actuators B Chem.* **149**, 325 (2010).

- ²¹C. Renault, X. Li, S. E. Fosdick, and R. M. Crooks, *Anal. Chem.* **85**, 7976 (2013).
- ²²P. A. Samant and M. R. Prausnitz, *Proc. Natl. Acad. Sci. U. S. A.* **115**, 4583 (2018).
- ²³D. P. Rose, M. E. Ratterman, D. K. Griffin, L. Hou, N. Kelly-Loughnane, R. R. Naik, J. A. Hagen, I. Papautsky, and J. C. Heikenfeld, *IEEE Trans. Biomed. Eng.* **62**, 1457 (2015).
- ²⁴A. Apilux, W. Dungchai, W. Siangproh, N. Praphairakshit, C. S. Henry, and O. Chailapakul, *Anal. Chem.* **82**, 51727 (2010).
- ²⁵J. L. Osborn, B. Lutz, E. Fu, P. Kauffman, D. Y. Stevens, and P. Yager, *Lab Chip* **10**, 2659 (2010).
- ²⁶A. R. Rezk, A. Qi, J. R. Friend, W. H. Li, and L. Y. Yeo, *Lab Chip* **12**, 773 (2012).
- ²⁷E. Elizalde, R. Urtega, and C. L. A. Berli, *Lab Chip* **15**, 2173 (2015).
- ²⁸X. Wang, J. A. Hagen, and I. Papautsky, *Biomicrofluidics* **7**, 014107 (2013).
- ²⁹S. Choi, S.-K. Kim, G.-J. Lee, and H.-K. Park, *Sens. Actuators B Chem.* **219**, 245 (2015).
- ³⁰D. Sechi, B. Greer, J. Johnson, and N. Hashemi, *Anal. Chem.* **85**, 10733 (2013).
- ³¹B. M. Cummins, R. Chinthapatla, B. Lenin, F. S. Ligler, and G. M. Walker, *Technology* **05**, 21 (2017).
- ³²N. S. Lynn and D. S. Dandy, *Lab Chip* **9**, 3422 (2009).
- ³³N. Goeddecke, J. Eijkel, and A. Manz, *Lab Chip* **2**, 219 (2002).
- ³⁴Z.-R. Xu, C.-H. Zhing, Y.-X. Guan, X.-W. Chen, J.-H. Wang, and Z.-L. Fang, *Lab Chip* **8**, 1658 (2008).
- ³⁵L. Jingmin, L. Chong, X. Zheng, Z. Kaiping, K. Xue, and W. Lidong, *PLoS One* **7**, e50320 (2012).
- ³⁶S. Wong, M. Cabodi, J. Rolland, and C. Klapperich, *Anal. Chem.* **86**, 11981 (2014).
- ³⁷X. Huang, Y. Liu, K. Chen, W.-J. Shin, C.-J. Lu, G.-W. Kong, D. Patnaik, S.-H. Lee, J. F. Cortes, and J. A. Rogers, *Small* **10**, 3083 (2010).
- ³⁸A. Koh, D. Wang, Y. Xue, S. Lee, R. M. Pielak, J. Kim, T. Hwang, S. Min, A. Banks, P. Bastien, M. C. Manco, L. Wang, K. R. Ammann, K.-I. Jang, P. Won, S. Han, R. Ghaffari, U. Paik, M. J. Slepian, G. Balooch, Y. Huang, and J. A. Rogers, *Sci. Transl. Med.* **8**, 366ra165 (2016).
- ³⁹J. Choi, D. Kang, S. Han, S. B. Kim, and J. A. Rogers, *Adv. Healthc. Mater.* **6**, 1 (2017).
- ⁴⁰W. Gao, S. Emaminejad, H. Y. Y. Nyein, S. Challa, K. Chen, A. Peck, H. M. Fahad, H. Ota, H. Shiraki, D. Kiriya, D.-H. Lien, G. A. Brooks, R. W. Davis, and A. Javey, *Nature* **529**, 509 (2016).
- ⁴¹T. Shay, M. D. Dickey, and O. D. Velev, *Lab Chip* **17**, 710 (2017).
- ⁴²A. Alizadeh, A. Burns, R. Lenigk, R. Gettings, J. Ashe, A. Porter, M. McCaul, R. Barrett, D. Diamond, P. White, P. Sneath, and M. Tomczak, *Lab Chip* **18**, 2632 (2018).
- ⁴³Y. Zhang, H. Guo, S. B. Kim, Y. Wu, D. Ostojich, S. H. Park, X. Wang, Z. Weng, R. Li, A. J. Bandodkar, R. Ghaffari, and J. A. Rogers, *Lab Chip* **19**, 1545 (2019).
- ⁴⁴S. B. Kim, K. H. Lee, M. S. Raj, B. Lee, J. T. Reeder, J. Koo, A. Hourlier-Fargette, A. J. Bandodkar, S. M. Won, Y. Sekine, J. Choi, Y. Zhang, J. Yoon, B. H. Kim, Y. Yun, S. Lee, J. Shin, J. Kim, R. Ghaffari, and J. A. Rogers, *Small* **14**, 1802876 (2018).
- ⁴⁵A. Hauke, P. Simmers, Y. R. Ojha, B. D. Cameron, R. Ballweg, T. Zhang, N. Twine, M. Brothers, E. Gomez, and J. Heikenfeld, *Lab Chip* **18**, 3750 (2018).
- ⁴⁶P. Ray and A. J. Steckl, *ACS Sens.* **4**, 1346 (2019).
- ⁴⁷Y. Sekine, S. B. Kim, Y. Zhang, A. J. Bandodkar, S. Xu, J. Choi, M. Irie, T. R. Ray, P. Kohli, N. Kozai, T. Sugita, Y. Wu, K. H. Lee, K.-T. Lee, R. Ghaffari, and J. A. Rogers, *Lab Chip* **18**, 2178 (2018).
- ⁴⁸P. M. van Kemenade, M. M. J. Houben, J. M. Huyghe, and L. F. A. Douven, *Ski. Res. Technol.* **10**, 109 (2004).
- ⁴⁹F. J. Zhao, M. Bonmarin, Z. C. Chen, M. Larson, D. Fay, D. Runnoe, and J. Heikenfeld, *Lab Chip* **20**, 168 (2020).
- ⁵⁰H. Darcy, *Les Fontaines Publiques de la Ville de Dijon: Exposition et Application des Principes à Suivre et des Formules à Employer Dans les Questions de Distribution D'eau* (Dalmont, 1856).
- ⁵¹S. Mendez, E. M. Fenton, G. R. Gallegos, D. N. Petsev, S. S. Sibbett, H. A. Stone, Y. Zhang, and G. P. Lopez, *Langmuir* **26**, 1380 (2009).
- ⁵²V. A. Jambhekar, R. Helmig, N. Schröder, and N. Shokri, *Transp. Porous Media* **110**, 251 (2015).
- ⁵³Z. Sonner, E. Wilder, J. Heikenfeld, G. Kasting, F. Beyette, D. Swaile, F. Sherman, J. Joyce, J. Hagen, N. Kelley-Loughnane, and R. Naik, *Biomicrofluidics* **9**, 031301 (2015).
- ⁵⁴A. J. Bandodkar, P. Gutruf, J. Choi, K. H. Lee, Y. Sekine, J. T. Reeder, W. J. Jeang, A. J. Aranyosi, S. P. Lee, J. B. Model, R. Ghaffari, C.-J. Su, J. P. Leshock, T. Ray, A. Verrillo, K. Thomas, V. Krishnamurthi, S. Han, J. Kim, S. Krishnan, T. Hang, and J. A. Rogers, *Sci. Adv.* **5**, eaav3294 (2019).
- ⁵⁵J. Choi, A. J. Bandodkar, J. T. Reeder, T. R. Ray, A. Turnquist, S. B. Kim, N. Nyberg, A. H. Fargette, J. B. Model, A. J. Aranyosi, X. Xu, R. Ghaffari, and J. A. Rogers, *ACS Sens.* **4**, 379 (2019).
- ⁵⁶J. T. Reeder, J. Choi, Y. Xue, P. Gutruf, J. Hanson, M. Liu, T. Ray, A. J. Bandodkar, R. Avila, W. Xia, S. Krishnan, S. Xu, K. Barnes, M. Pahnke, R. Ghaffari, Y. Huang, and J. A. Rogers, *Sci. Adv.* **5**, eaau6356 (2019).
- ⁵⁷H. Y. Y. Nyein, L.-C. Tai, Q. P. Ngo, M. Chao, G. B. Zhang, W. Gao, M. Bariya, J. Bullock, H. Kim, H. M. Fahad, and A. Javey, *ACS Sens.* **2**, 1860 (2017).
- ⁵⁸J. Kim, I. Jeerapan, S. Imani, T. N. Cho, A. Bandodkar, S. Cinti, P. P. Mercier, and J. Wang, *ACS Sens.* **1**, 1011 (2016).
- ⁵⁹Z. Sonner, E. Wilder, T. Gaillard, G. Kasting, and J. Heikenfeld, *Lab Chip* **17**, 2550 (2017).
- ⁶⁰M. A. Yokus, T. Saha, J. Fang, M. D. Dickey, O. D. Velev, and M. A. Daniele, in *2019 IEEE SENSORS* (IEEE, 2019), pp. 1–4.